Regular Article

ANALYTICAL AND BIOANALYTICAL CHEMISTRY RESEARCH

Published by the Iranian Chemical Society

Anal. Bioanal. Chem. Res., Vol. 9, No. 1, 21-31, January 2022.

Polyamidoamine Dendrimers-MoS_2 Nanocomposites for Photocatalytic Degradation of Chlorpyrifos and Glyphosate Pesticides

Arman Mohammadi[a,b] and Mehdi Shahmirzaei[c,*]

[a]*Department of Chemistry, Shahid Bahonar University of Kerman, Kerman, Iran*

[b]*Young Researchers Society, Shahid Bahonar University of Kerman, Iran*

[c]*Department of Metallurgy Engineering, Payame Noor University (PNU), P. O. Box: 19395-3697, Tehran, Iran*

(Received 5 February 2021 Accepted 8 August 2021)

Polyamidoamine dendrimer functionalized with MoS_2 nanoparticles was synthesized and fully characterized using field-emission scanning electron microscopy, energy-dispersive X-ray spectroscopy, Fourier-transform infrared spectroscopy, X-ray diffractometry, Brunauer-Emmett-Teller, and thermal gravimetric analysis. The synthesized nanocomposite showed excellent photocatalytic activities for the degradation of two commonly used pesticides (chlorpyrifos and glyphosate). According to the optimization study, the pH value of 10 and the minimum reaction time of 110 min were required for optimal degradation of pesticides. Based on the kinetic study of the photocatalytic reaction, it was inferred that more than 95% of the pesticides were degraded into non-harmful products in less than two hours. By comparing the obtained data in this study with previous reports for photocatalytic degradation of chlorpyrifos and glyphosate, it was concluded that the present nanocomposite was able to degrade pesticides faster and more efficient than available catalysts.

Keywords: Chlorpyrifos, Glyphosate, Polyamidoamine dendrimer, Photocatalyst, Pesticide

INTRODUCTION

Enormous amounts of pesticides and fertilizers are used every day due to industrial agriculture and the present demand for increasing global food production. Synthetic pesticides have a crucial role in the food production chain by reducing the crop losses up to 30% for major crops cultivated on earth [1-3]. Despite their positive roles, pesticides negatively affect the environment, including soil, water bodies, and the atmosphere [4-6]. Improper usage of pesticides has lethal effects on human life and could damage the respiratory system, kidneys, and DNA and cause diabetes, Parkinson's, and other chronic disorders [7-10]. In this regard, there is a considerable demand for pesticide removal and remediation from the environment. Several chemical and biological approaches have been implemented, including pesticide immobilization, nanofiltration, electro-kinetic remediation, advanced oxidation process, and bioremediation techniques [11-15]. In addition to their low efficiency for pesticide removal, these techniques suffer from high cost and production of secondary toxic pollutants [16-18].

Recently, photocatalytic degradation of pesticides has endeavored as an emerging technology for efficient and green pesticide removal. Meanwhile, photocatalytic degradation of pesticides based on nanostructures is in the center of attention due to their ability to decompose the organic pollutants completely and with minimum secondary harmful substances [19-21]. In this regard, different nanostructures have been exploited to degrade pesticides in the presence of UV or visible light, depending on their optoelectronic properties.

For instance, TiO_2 [22], ZnO [23], g-C_3N_4 [24], Fe_3O_4/$BiVO_4$ [25], magnetic graphene oxide@MIL-101(Fe) [26], and many other metal oxide nanoparticles and nanocomposites have been used for the degradation of

*Corresponding author. E-mail: m.shahmirzaei@pnu.ac.ir

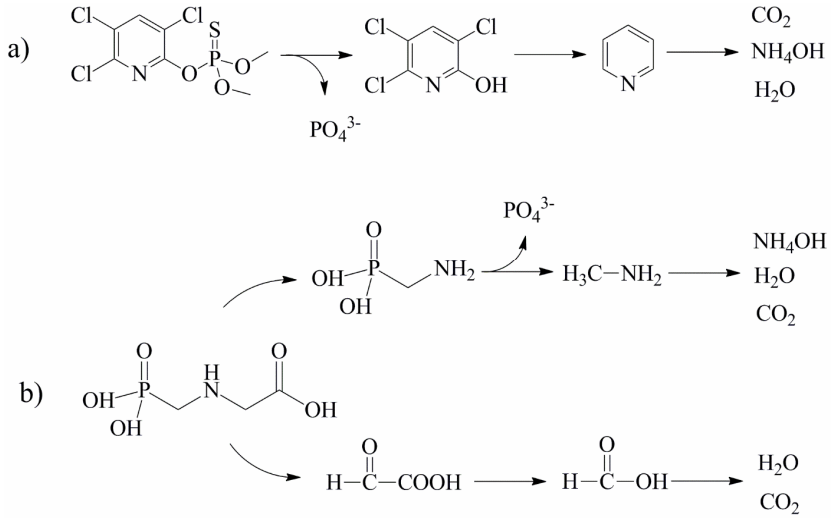

Scheme 1. A possible mechanism for degradation of (a) chlorpyrifos and (b) glyphosate pesticides

imidacloprid, chlorinated pesticides, monocrotophos pesticide, diazinon, atrazine, and other commonly used pesticides.

In this study, the polyamidoamine dendrimer (PAMAM)-grafted MoS_2 nanoparticles have been successfully synthesized to take advantage of excellent photocatalytic behavior for degradation of chlorpyrifos and glyphosate pesticides under visible light (Scheme 1). This is the first report on the application of MoS_2-PAMAM nanocomposites for photocatalytic degradation of pesticides to the best of our knowledge. According to the obtained results after a complete optimization of the experimental parameters, the prepared nanocomposite showed outstanding performance for fully decomposing the studied pesticides to non-harmful compounds. This research can pave the way for further studies in photocatalytic nanostructures to eliminate the chemical pesticides from the aqueous environment.

EXPERIMENTAL

Chemicals and Materials

All of the chemicals used for the synthesis of PAMAM such as diethylenetriamine ($(NH_2CH_2CH_2)_2NH$ with molecular weight 103.17 and purity ≥ 99%), methyl acrylate (CH_2=$CHCOOCH_3$ with molecular weight 86.09 and purity ≥ 99.5%), and ethylenediamine ($NH_2CH_2CH_2NH_2$ with molecular weight 60.10 and purity ≥ 99.5%) were purchased from Merck (Darmstadt, Germany). Sodium molybdate (Na_2MoO_4, 99%), methanol, and thiourea were purchased from Sigma-Aldrich (Steinheim, Germany). CO_2-free water, ethanol, sodium hydroxide, acetic acid, sulfuric acid, hydrochloric acid, dimethyl sulfoxide, and dichloromethane were purchased from Sigma-Aldrich (Steinheim, Germany).

Characterizations

Morphological features of the obtained nanostructures were characterized using field-emission scanning electron microscopy (FE-SEM, Sigma VP, ZEISS) and transmission electron microscopy (TEM, EM10C, 100 kV, ZEISS). Fourier-transform infrared spectroscopy (FT-IR) was performed on a Cary 630 spectrophotometer, equipped with a single reflection diamond (attenuated total reflectance) ATR sample interface. Compositional analysis was done using an X-ray diffraction unit (Panalytical PW-1700) using Cu-Kα irradiation. UV-Vis spectroscopy (UNICO, Germany) was used for determining the concentration of pesticides at specific wavelengths (230 and 290 nm for chlorpyrifos and 260 and 360 nm for glyphosate). Nitrogen adsorption/desorption studies were done by a computer-interfaced Nova 3200 series instrument (Quantachrgme, USA) using Brunauer-Emmett-Teller (BET) determining the surface area. Thermogravimetric analysis (TGA) was

performed by NETZCH STA 309 PC/PG under nitrogen atmosphere with a flow rate of 60 ml min^{-1}, heating rate at 10 °C min^{-1} from 25 to 1000 °C.

Synthesis of Modified Dendrimer (PAMAM) by MoS_2 Nanoparticles

The typical procedure for the preparation of PAMAM dendrimer. The PAMAM dendrimer was synthesized according to the following procedure [27]. At first, 1 g of diethylenetriamine was dissolved in 5 ml of methanol under a nitrogen gas atmosphere and stirring at room temperature (25 °C). Then, 10 g of methyl acrylate was dissolved in 25 mL of methanol and added dropwise to the diethylenetriamine solution. The reaction mixture was stirred for seven days under a nitrogen gas atmosphere at room temperature (25 °C). After the reaction completion and evaporation of all volatile compounds using a vacuum pump, the 0.5-generation PAMAM dendrimer (G0.5) with $-OCH_3$ terminated groups was obtained. Afterward, under nitrogen gas atmosphere at room temperature (25 °C), 40 ml of ethylenediamine was dissolved in 20 ml of methanol and added to the G0.5 solution. After stirring for another seven days under a nitrogen gas atmosphere at room temperature, the first generation of dendrimer (G1) with terminated groups of $-NH_2$ was obtained. For further growth of the dendrimer, 15 ml of methyl acrylate was added to 3.37 g of G1 solution and stirred for seven days under a nitrogen gas atmosphere, and a viscous, yellowish liquid with terminated groups of 10-arm-OCH_3 was obtained (G1.5). By repeating the procedure mentioned above for G 1.5 solution using 30 ml of ethylenediamine, the next generation of dendrimer was obtained with 10-NH_2 terminal groups (G2).

Immobilization of the MoS_2 nanoparticles. Modified PAMAM by MoS_2 was prepared by the chemical reduction method. At first, 25 ml of PAMAM solution was added to the deionized water (25 ml) under vigorous magnetic stirring (1000 rpm) and nitrogen gas atmosphere. Then, 1.08 g sodium molybdate and 1.02 g thiourea were added to this solution and dispersed by vigorous magnetic stirring (1000 rpm) under a nitrogen gas atmosphere for 24 h. Afterward, this solution was transferred to a 100 ml Teflon-lined steel autoclave and placed at 70 °C for 24 h. After the immobilization process, the PAMAM containing MoS_2 nanoparticles was separated from the reaction mixture by centrifugation at 4000 rpm for 10 min, and finally, the supernatant was decanted. The obtained gel was washed three times with ethanol (10 ml) and deionized water (10 ml). The MoS_2-PAMAM nanocomposite was obtained after drying at 50 °C for 24 h [28]. It should be mentioned that a complete synthesis of PAMAM polymer and its functionalization with MoS_2 nanoparticles would take several weeks.

Photocatalytic Activities

The photocatalytic activity of MoS_2-PAMAM nanocomposite was studied in the presence of chlorpyrifos and glyphosate pesticides under visible light *via* a 250 W tungsten lamp. For a typical experiment, a specific amount of MoS_2-PAMAM nanocomposite was added to freshly prepared chlorpyrifos and glyphosate pesticide solutions (20 mg l^{-1} in 20 ml DI water) and kept stirring for 120 min. After completion the reactions, the photocatalysts were separated using centrifugation and washed several times with ethanol and DI water. The degradation amount of pesticides were estimated using a UV-Vis spectrophotometer. It should be mentioned that the Glyphosate pesticides do not have any chatachteristic peak in the UV-Vis spectra and the concentration of PO_4^{3-} should be measured using Mo-Sb-ascorbic acid colorimetric method [21].

RESULTS AND DISCUSSION

Characterization of the Synthesized MoS_2-PAMAM Nanocomposites

The structure and morphology of the MoS_2-PAMAM nanocomposite were characterized using FE-SEM and TEM microscopies (Fig. 1). According to the SEM results (Figs. 1a and 1b), uniform sphere-like MoS_2 NPs with an average size of 23 nm can be seen on PAMAM nanocomposites. The monodispersity of the obtained spherical MoS_2 NPs was also confirmed by TEM observations (Figs. 1c and 1d). Besides, the EDS-mapping analysis of the MoS_2-PAMAM nanocomposites shows a homogeneous distribution of elements of Mo, S, C, N, and O (Figs. 1e and 1f).

FT-IR spectroscopy was carried out to characterize the

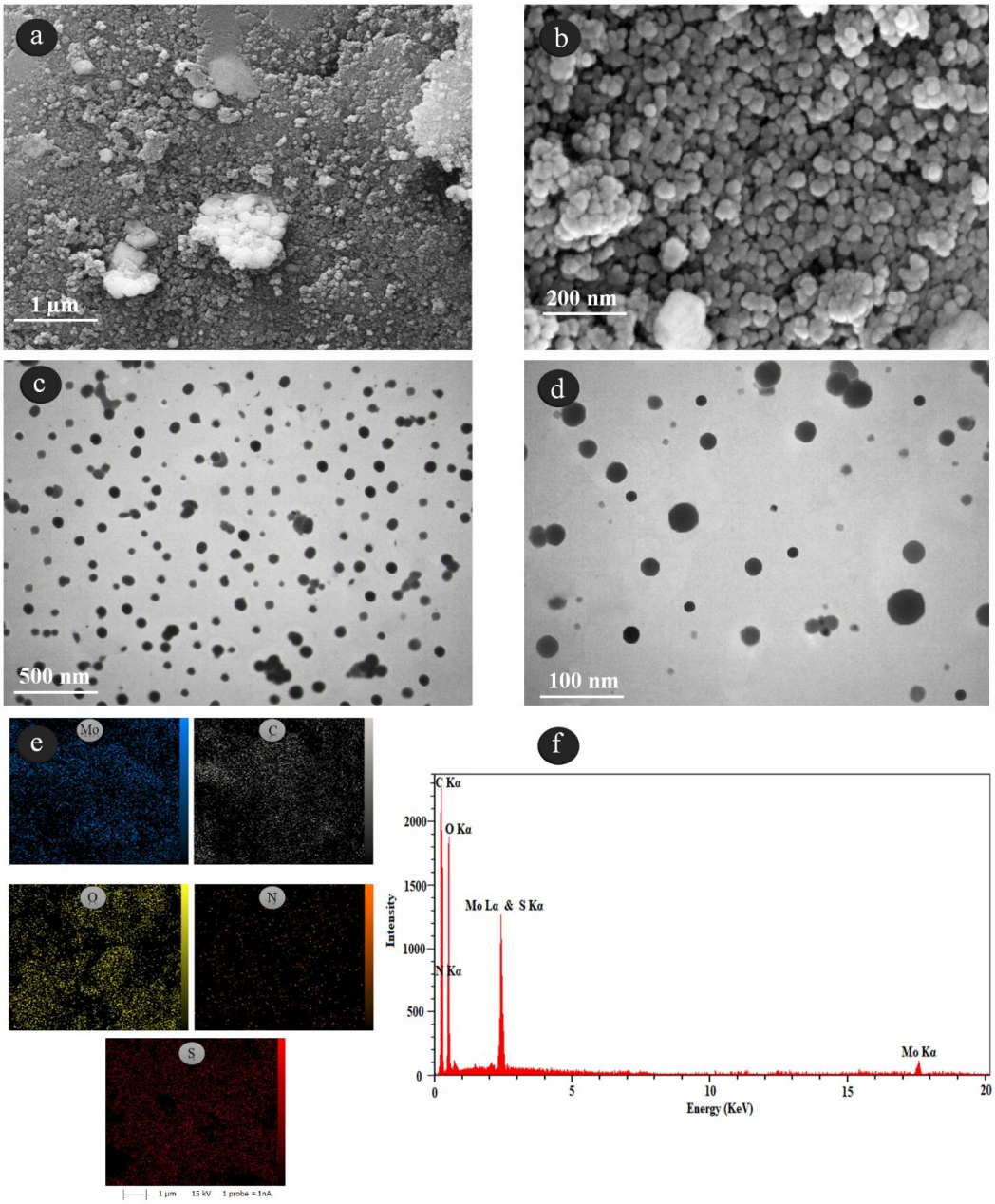

Fig. 1. Morphological and elemental analysis of the synthesized MoS_2-PAMAM nanocomposite. Scanning electron microscopy images (a and b), and transmission electron microscopy images (c and d). (e) and (f) show the EDS map and spectra of the synthesized MoS_2-PAMAM nanocomposite.

functional groups on the PAMAM and MoS_2-PAMAM nanocomposites. According to the obtained data (Fig. 2a), the broadband at 3468 cm^{-1} and the double peaks around 2700-3000 cm^{-1} can be attributed to the OH and N-H stretching vibration of the PAMAM, respectively. Moreover, a peak located at 1713 cm^{-1} could be assigned to the C=N vibration of the PAMAM. The absorption peaks at 1648 and 1058 cm^{-1} were assigned to the stretching

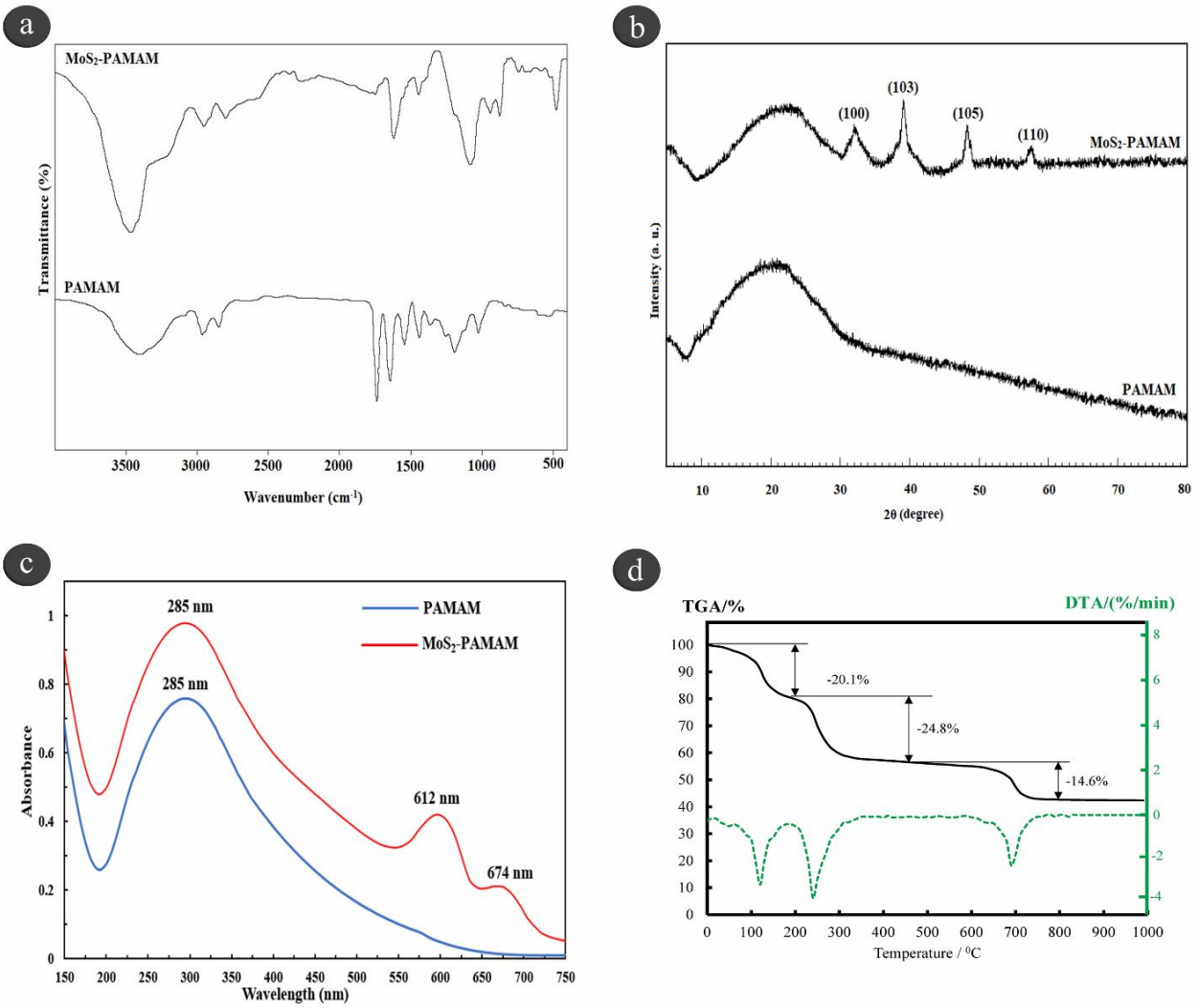

Fig. 2. Optical, compositional, and thermal analysis of MoS_2-PAMAM nanocomposites in comparison with PAMAM. (a), (b), (c), and (d) show the FTIR spectra, XRD pattern, UV-Vis spectra, and TGA curve of MoS_2-PAMAM nanocomposites in comparison to PAMAM.

vibration of the C=O=O bond of amide and C=C bond in the PAMAM, respectively. As it can be seen in Fig. 2a, incorporation of MoS_2 nanoparticles into the PAMAM structure resulted in significant changes in peak intensities, especially at 486 cm^{-1} and its shoulder around 512 $cm^{-1,}$ which are related to the S-H vibrations and strong S-S bond in MoS_2 structure [29,30].

The crystalline structure of the PAMAM and MoS_2-PAMAM nanocomposites was investigated using XRD measurements (Fig. 2b). The amorphous nature of PAMAM can be seen from the background of the XRD pattern. The diffraction peaks in the XRD pattern of MoS_2-PAMAM nanocomposites at 2θ = 32°, 40°, 48°, and 57° correspond to the (100), (103), (105), and (110) planes, which are very close to the standard patterns of the crystalline MoS_2 nanoparticle [31,32]. The UV-Vis spectra of PAMAM dendrimer and MoS_2-PAMAM nanocomposite are shown in Fig. 2c. According to the obtained data, three distinct peaks at 285 nm, 612 nm, and 674 nm can be seen for MoS_2-PAMAM nanocomposite. The XRD pattern and UV-Vis

spectra of the MoS_2-PAMAM with distinct peaks at 612 nm and 674 nm confirmed nanocomposites' successful formation [33]. TGA evaluated the thermal stability of MoS_2-PAMAM under the air atmosphere, and according to the obtained results (Fig. 2d), 50 wt% total weight loss was observed for MoS_2-PAMAM nanocomposite when heated to 1000 °C. Evaporation of water and organic compounds was initiated at 100-150 °C, with a total weight loss of 20.1%. The 24.8% mass loss observed at 200-250 °C can be attributed to the PAMAM oxidation. The final decomposition (14.6%) occurred at 600-700 °C, where the MoS_2 decomposed to molybdenum oxide and sulfur dioxide under the air atmosphere [34].

The nitrogen sorption isotherm of PAMAM and MoS_2-PAMAM nanocomposites followed the type IV adsorption isotherm according to the IUPAC classification [35]. In addition, the BET surface area, BJH desorption volume of the pore, and desorption average pore diameter were measured as 12.8 m^2 g^{-1}, 3.08 cm^3 g^{-1}, and 9.14 nm, respectively (Fig. 3). The MoS_2-PAMAM nanocomposite showed a pronounced increase in the pore size and the surface area compared to the sole PAMAM. This behavior suggests that MoS_2 nanoparticles increased the relative surface area and enabled the synergistic effect on the catalytic activity of the MoS_2-PAMAM nanocomposite.

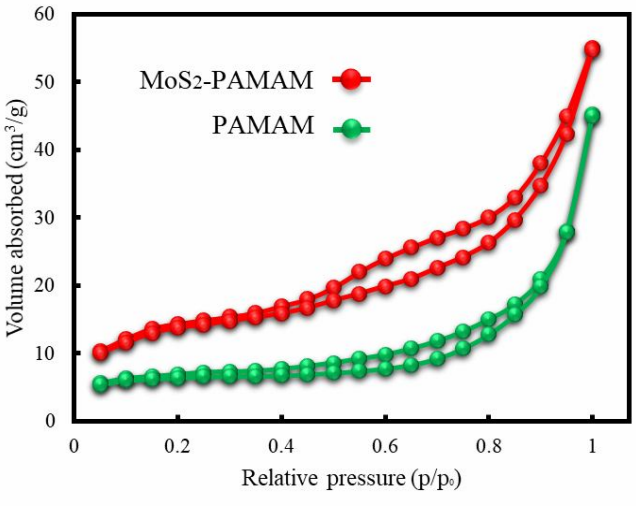

Fig. 3. The nitrogen adsorption isotherm of PAMAM and MoS_2-PAMAM nanocomposites.

Application of MoS_2-PAMAM Nanocomposite for Catalytic Degradation of Pesticides

Effect of pesticides concentration. The catalytic activity of MoS_2-PAMAM nanocomposite for degradation of organophosphorus pesticides (chlorpyrifos and glyphosate) was studied according to the mentioned protocol in section 2.4. According to the obtained data, by changing the initial concentrations of chlorpyrifos and glyphosate pesticides from 1 ppm to 20 ppm, the degradation percentage gradually decreased from 97% to 73% for chlorpyrifos and 96% to 61% for glyphosate (Fig. 4a). The percentage of degradation was relevant to the number of OH radicals available on the surface of the MoS_2-PAMAM nanocomposite surface and their ability to react with the pesticide molecules. It is worth mentioning that a high concentration of pesticides would cover the surface of MoS_2-PAMAM nanocomposite and decrease the efficiency of reaction due to steric effects [36].

Effect of illumination time. When the experiment was done in the dark condition, the degradation efficiency of chlorpyrifos and glyphosate pesticides decreased to 27% and 22% in 20 min, respectively. It can be inferred that the photocatalytic activity of MoS_2-PAMAM nanocomposite plays a crucial role in the visible-light-induced degradation of pesticides. According to the obtained data in Fig. 4b, more than 70 wt% of the pesticides were degraded in the first 20 min, confirming the fast reaction kinetics between MoS_2-PAMAM nanocomposite and the pesticides.

Effect of pH. Figure 4c shows that the solution's pH has a significant effect on the degradation efficiency of pesticides. The crucial role of pH can be attributed to its effect on the molecules' surface charge, which can hinder or facilitate the chemical reaction between species at the surface [37]. According to the obtained data, at a pH value of 10, more than 90% of the pesticides were degraded using MoS_2-PAMAM nanocomposite. According to the pKa values of chlorpyrifos and glyphosate, at pH values in the range of 5-10, both of the pesticides have negative charges so they readily interact with positive charged MoS_2-PAMAM nanocomposite.

According to the obtained data, the optimal values (pH = 10 and 110 min for reaction time) were used for further experiments.

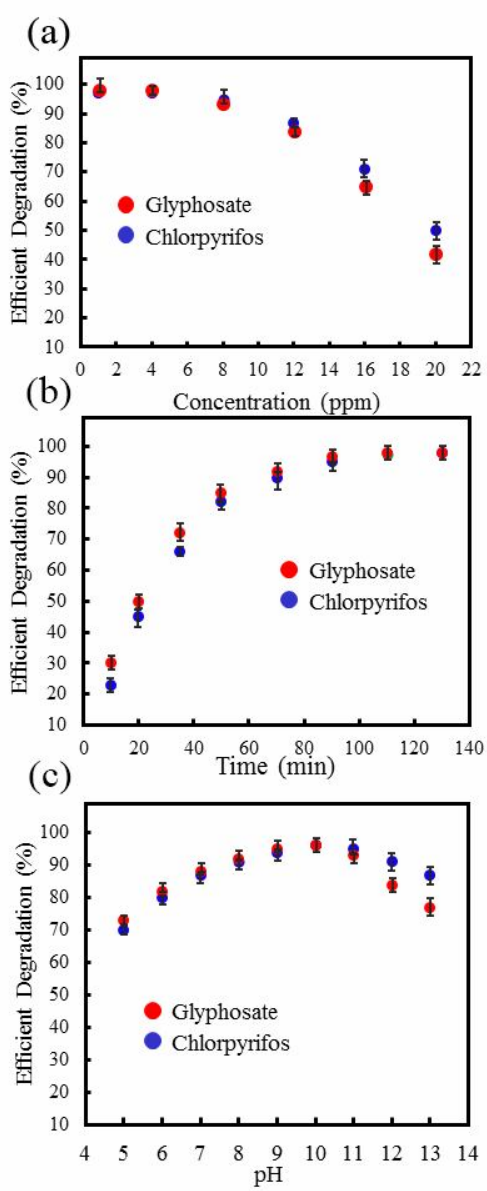

Fig. 4. The effects of pesticide concentration (a), reaction time (b), and pH (c) on the degradation efficiency of chlorpyrifos and glyphosate using MoS_2-PAMAM nanocomposite as the photocatalyst. In panel (a) the pH of the solution and the reaction time were kept constant at 10 and 110 mins, respectively. In panel (b) the pH of the solution and the pesticides concentration were kept constant at 10 and 4 ppm, respectively. In panel (c) the reaction time and the concentration of pesticides were kept constant at 110 mins and 4 ppm, respectively.

The role of MoS_2 nanoparticles. The role of MoS_2 nanoparticle for photocatalytic degradation of pesticides was studied by evaluating the efficiency of degradation for both PAMAM and MoS_2-PAMAM in light-off and light-on conditions. According to the obtained data, as long as the reaction was in the dark condition, no reaction took place even in the presence of MoS_2 nanoparticles (Fig. 5a). On the other hand, as soon as the tungsten lamp turned on, the reaction started to proceed and in the presence of MoS_2-PAMAM nanocomposite, more than 95% of the pesticides were degraded in less than 2 h (Fig. 5b). In the case of pristine PAMAM, the maximum value of 75% and 79% can be obtained for the degradation of chlorpyrifos and glyphosate, respectively. The significant changes in the UV-Vis spectra (Figs. 5c and d) clearly shows the degradation of pesticides in the period of 0-110 min. It should be mentioned that, upon the iridation of MoS_2-PAMAM nanocomposite, the photogenerated positive holes from the valence band rapidly react with water molecoules to produce hydroxyl radicals which are responsible for degradation of pesticides.

Reusability. The catalyst's reusability was studied using a specific amount of MoS_2-PAMAM nanocomposite for six successive runs and monitoring the efficiency of each run using a UV-Vis spectroscopy. According to the obtained data in Fig. 6, the photocatalyst efficiency was decreased from 97% to 82% and 81% after six successive runs for degradation of glyphosate and chlorpyrifos, respectively. This can be inferred that the synthesized MoS_2-PAMAM nanocomposite could be used for photocatalytic degradation of chlorpyrifos and glyphosate without a significant drop in its efficiency.

Reaction Kinetics Study

In order to study the kinetics of the degradation, the reaction completion was carefully studied in different time intervals for both pesticides. According to the obtained data (Fig. 7a), degradation of both pesticides follow the pseudo-second-order model. The Langmuir-Hinshelwood model [38] was used to model the degradation kinetic as follows:

$$Ln\left(\frac{C}{C_0}\right) = Ln\left(\frac{A}{A_0}\right) = kt \qquad (1)$$

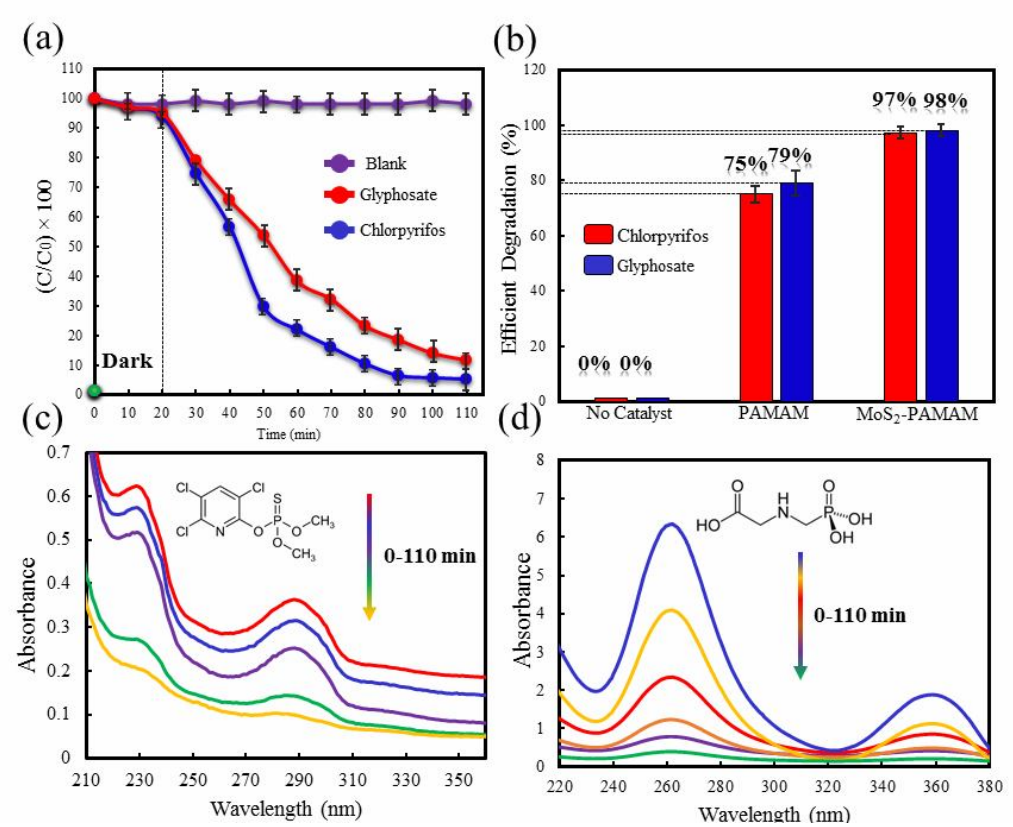

Fig. 5. (a) and (b) degradation efficiency of chlorpyrifos and glyphosate in the presence of PAMAM and MoS_2-PAMAM nanocomposites. (c) and (d) show the changes in UV-Vis spectra in the period of 0-110 min for chlorpyrifos and glyphosate, respectively. All of the parameters except time were in optimal condition (pH = 10, concentration of pesticides = 4 ppm).

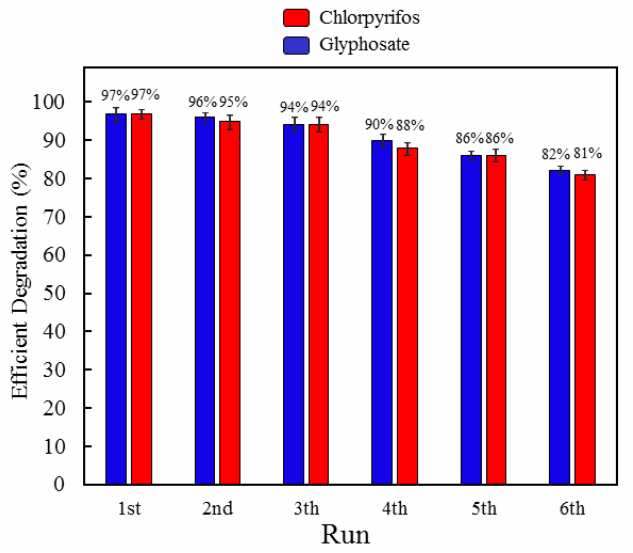

Fig. 6. The degradation efficiency of chlorpyrifos and glyphosate pesticides using MoS_2-PAMAM nanocomposite as the photocatalyst.

C_0 is the initial concentration of the pesticides, and C is the actual pesticide concentration at the time = t. According to the fitted data in Fig. 7b, both regression values showed that the reaction kinetics for photocatalytic degradation of pesticides follow the pseudo-second-order model. In Table 1, the photocatalytic activity of the synthesized MoS_2-PAMAM nanocomposite was compared with previously reported catalysts for the degradation of chlorpyrifos and glyphosate pesticides. According to the data, the rate constant of the fabricated MoS_2-PAMAM nanocomposite for the degradation of chlorpyrifos and glyphosate pesticides is superior or comparable with other nanocomposites. So, the rapid degradation of pesticides using the developed nanocomposite is the main advantage of this study. Based on the absorbance measurement for chlorpyrifos and glyphosate pesticides at 290 nm and 260 nm, the LOD values of 0.34 ppm and 1.93 ppm were

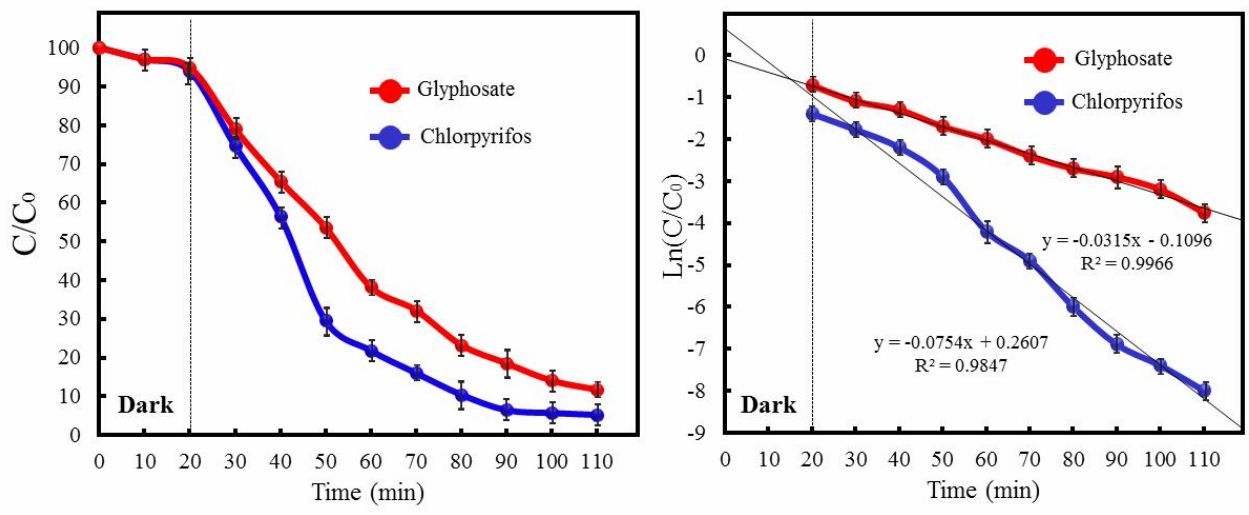

Fig. 7. Kinetics of the photocatalytic reaction completion for degradation of chlorpyrifos (blue dots) and glyphosate (red dots) in the presence of MoS_2-PAMAM nanocomposite.

Table 1. Comparison the Previously Reported Catalysts with those Obtained in this Study for the Degradation of Chlorpyrifos and Glyphosate

Catalyst	The rate constant ($\times 10^{-2}$ (min))	Pesticide	Ref.
TiO_2	6.00	Chlorpyrifos	[39]
Th^{4+} doped TiO_2	1.82		[40]
Mo^{6+} doped TiO_2	2.20		[40]
MoS_2-PAMAM	7.54		This study
TiO_2/silica gel	1.85	Glyphosate	[41]
SnO_2-TiO_2	6.10		[42]
In_2S_3/$BiVO_4$	0.81		[43]
MoS_2-PAMAM	3.15		This study

obtained, respectively. The linear dynamic ranges for chlorpyrifos and glyphosate pesticides were calculated as 10-50 ppm and 5-25 ppm, respectively.

CONCLUSIONS

In this study, MoS_2-PAMAM nanocomposite was synthesized by the hydrothermal approach and fully characterized using XRD, electron microscopies, optical spectroscopies, and thermal analysis. XRD pattern confirmed the formation of MoS_2 nanoparticles, and SEM images show that the MoS_2 nanoparticles are monodispersed and well-distributed throughout the PAMAM matrix. The synthesized MoS_2-PAMAM nanocomposite showed excellent photocatalytic activities for the degradation of two commonly used pesticides under visible light. In the presence of synthesized nanocomposite, chlorpyrifos and glyphosate pesticides were degraded with efficiencies more than 95% in less than two hours. Kinetics of the reaction and the effects of pertinent factors (*e.g.,* pH,

reaction time, and concentration of pesticides) were fully discussed. According to the obtained data, MoS_2-PAMAM nanocomposite could be an efficient photocatalysis for other pesticides or chemical toxins.

REFERENCES

[1] S. Savary, L. Willocquet, S. Pethybridge, P. Esker, N. McRoberts, A. Nelson, Nat. Ecol. Evol. 3 (2019) 430.

[2] M. Heydari, A. Amirjani, M. Bagheri, I. Sharifian, Q. Sabahi, Environ. Sci. Pollut. Res. 27 (2019) 6667.

[3] B. Tiwari, S. Kharwar, D. Tiwari (Eds.), Cyanobacteria. From Basic Science to Applications. Elsevier, 2019, p. 303.

[4] K. Rajmohan, R. Chandrasekaran, S. Varjani, Indian. J. Microbiol. 60 (2020) 125.

[5] M. Agostini, I. Roesler, C. Bonetto, A. Ronco, D. Bilenca, Biol. Conservat. 241 (2020) 108355.

[6] J. Everett, PLoS ONE 8 (2013) e82131.

[7] A. Sabarwal, K. Kumar, R. Singh, Environ. Toxicol. Pharmacol. 63 (2018) 103.

[8] A. Tsatsakis, N. Tyshko, A. Docea, S. Shestakova, Y. Sidorova, N. Petrov, O. Zlatian, M. Mach, T. Hartung, V. Tutelyan, Toxicol. Lett. 315 (2019) 96.

[9] A. Tsatsakis, A. Docea, D. Calina, A. Buga, O. Zlatian, S. Gutnikov, R. Kostoff, M. Aschner, Food. Chem. Toxicol. 125 (2019) 141.

[10] G. Weis, C. Assmann, F. Cadoná, B. Bonadiman, A. Alves, A. Machado, M. Duarte, I. da Cruz, I. Costabeber, Ecotoxicol. Environ. Saf. 182 (2019) 109420.

[11] S. Xue, J. Li, L. Zhou, J. Gao, G. Liu, L. Ma, Y. He, Y. Jiang, J. Agric. Food Chem. 67 (2019) 13518.

[12] E. Novotny, D. Murphy, H. Stefan, Sci. Total. Environ. 406 (2008) 131.

[13] H. Qin, W. Guo, X. Huang, P. Gao, H. Xiao, J. Eur. Ceram. Soc. 40 (2020) 145.

[14] M. Malakootian, A. Shahesmaeili, M. Faraji, H. Amiri, S. Silva Martinez, Process. Saf. Environ. Prot. 134 (2020) 292.

[15] T. Pham, H. Bui, T. Bui, Curr. Dev. Biotechnol. Bioeng. (2020) 309.

[16] F. Suanon, L. Tang, H. Sheng, Y. Fu, L. Xiang, Z. Wang, X. Shao, D. Mama, X. Jiang, F. Wang, J. Hazard. Mater. 393 (2020) 122388.

[17] H. Chen, S. Yu, X. Shen, D. Chen, X. Qiu, C. Song, C. Ding, Microb. Pathog. 51 (2011) 285.

[18] N. Firouzsalari, M. Shakerkhatibi, M. Pourakbar, A. Yadeghari, G. Safari, P. Sarbakhsh, J. Water. Process. Eng. 29 (2019) 100793.

[19] S. Kanan, M. Moyet, R. Arthur, H. Patterson, Catal. Rev. 62 (2019) 1.

[20] G. Luna-Sanguino, A. Ruíz-Delgado, A. Tolosana-Moranchel, L. Pascual, S. Malato, A. Bahamonde, M. Faraldos, Sci. Total. Environ. 737 (2020) 140286.

[21] D. Vaya, P. Surolia, Environ. Technol. Innovation. 20 (2020) 101128.

[22] A. Ismael, A. El-Shazly, S. Gaber, M. Rashad, A. Kamel, S. Hassan, RSC Adv. 10 (2020) 34806.

[23] N. Hanh, N. Le Minh Tri, D. Van Thuan, M. Thanh Tung, T. Pham, T. Minh, H. Trang, M. Binh, M. Nguyen, J. Photochem. Photobiol., A. 382 (2019) 111923.

[24] S. Ghodsi, A. Esrafili, R. Kalantary, M. Gholami, H. Sobhi, J. Photochem. Photobiol., A. 389 (2020) 112279.

[25] A. Kumar, Shalini, G. Sharma, M. Naushad, A. Kumar, S. Kalia, C. Guo, G. Mola, J. Photochem. Photobiol., A. 337 (2017) 118.

[26] H. Fakhri, M. Farzadkia, R. Boukherroub, V. Srivastava, M. Sillanpää, Solar Energy 208 (2020) 990.

[27] L. Thuy, S. Mallick, J. Choi, Int. J. Pharm. 492 (2015), 233.

[28] Y. Li, H. Wang, L. Xie, Y. Liang, G. Hong, H. Dai, J. Am. Chem. Soc. 133 (2011) 7296.

[29] L. Rosenberger, R. Baird, E. McCullen, G. Auner, G. Shreve, Surf. Interface. Anal. 40 (2008) 1254.

[30] H. Yang, J. Zhao, C. Wu, C. Ye, D. Zou, S. Wang, Chem. Eng. J. 351 (2018) 548.

[31] M. Hamblin, BBA Clinical 6 (2016) 113.

[32] M. Nemanashi, J. Noh, R. Meijboom, J. Mater. Sci. 53 (2018) 12663.

[33] D. Nimbalkar, H. Lo, P. Ramacharyulu, S. Ke, RSC Adv. 6 (2016) 31661.

[34] A. Raza, M. Ikram, M. Aqeel, M. Imran, A. Ul-Hamid, K. Riaz, S. Ali, Appl. Nanosci. 10 (2019) 1535.

[35] C. Buttersack, Phys. Chem. Chem. Phys. 21 (2019) 5614.
[36] M. Zangiabadi, A. Saljooqi, T. Shamspur, A. Mostafavi, Ceram. Int. 46 (2020) 6124.
[37] E. Murugan, J. Jebaranjitham, Chem. Eng. J. 259 (2015) 266.
[38] F. Soltani-nezhad, A. Saljooqi, T. Shamspur, A. Mostafavi, Polyhedron 165 (2019) 188.
[39] L. Devi, B. Murthy, S. Kumar, J. Mol. Catal. A: Chem. 308 (2009) 174.
[40] A. Amalraj, A. Pius, J. Water. Process. Eng. 7 (2015) 94.
[41] G. Echavia, F. Matzusawa, N. Negishi, Chemosphere 76 (2009) 595.
[42] P. Kongsong, L. Sikong, S. Niyomwas, V. Rachpech, Photochem. Photobiol. 90 (2014) 1243.
[43] Q. Tang, X. Luo, S. Yang, Y. Xu, Separ. Purif. Tech. 248 (2020) 117039.